Analyst

Accepted Manuscript

ROYAL SOCIETY OF CHEMISTRY

www.rsc.org/analyst

Analyst RSCPublishing

ARTICLE

Polydopamine-embedded $Cu_{2-x}Se$ nanoparticles as sensitive biosensing platform through the coupling of nanometal surface energy transfer and photo-induced electron transfer

Cite this: DOI: 10.1039/x0xx00000x

Received 00th January 2012,
Accepted 00th January 2012

DOI: 10.1039/x0xx00000x

www.rsc.org/

Hong Yan Zou,[ab] Peng Fei Gao,[a] Ming Xuan Gao[b] and Cheng Zhi Huang*[a,b],

Fully understanding and easy construction of specific biosensing principle is necessary for disease diagnostics and therapeutics in the hope to create new types of biosensors. Herein, we developed a new conceptual nanobiosensing platform by coupling nanometal surface energy transfer (NSET) and photo-induced electron transfer (PET) with polydopamine-embedded $Cu_{2-x}Se$ nanoparticles ($Cu_{2-x}SeNPs$@pDA) and DNA-conjugated fluorescent organic dyes. The new prepared $Cu_{2-x}SeNPs$@pDA has intense and broad localized surface plasmon resonance (LSPR) absorption over UV to near infrared (NIR) wavelengths, different affinity toward ssDNA versus dsDNA, and exhibits high multiplexed fluorescence quenching ability, and thus can act as acceptors in the energy transfer and electron transfer interactions between $Cu_{2-x}SeNPs$@pDA and fluorescent organic dyes. As a proof of concept, a new biosensing platform has been successfully developed for target biomacromolecules such as DNA and proteins, in which the NSET and PET interactions between $Cu_{2-x}SeNPs$@pDA and three different DNA-conjugated fluorescent dyes have been identified using steady-state and time-resolved fluorescence. A simple mathematical model was further applied to simulate the respective contributions of the coexisting NSET and PET to the total quenching observed for each DNA-conjugated dye in this sensing system. This study highlights the importance for understanding the coupling mechanistic details of NSET and PET processes, and the disclosed coupling mechanism of NSET and PET (NSET©PET) in the systems of $Cu_{2-x}SeNPs$@pDA with a wide wavelength range dyes provides new opportunities for sensitive biosensing applications.

Introduction

There has been an explosion of interest in the design of novel sensitive biosensing platform over the past two decades by coupling nanomaterials with biomolecular recognition events. Resonance energy transfer (RET) pairs participating in Förster resonance energy transfer (FRET),[1] plasma resonance energy transfer (PRET),[2] or nanometal surface energy transfer (NSET)[3] et al, and photo-induced electron transfer (PET) pairs,[4] have been inevitably involved in the biosensing upsurge. Nanomaterials such as gold nanoparticles,[5] SnO_2 nanoparticles,[6] polydopamine nanospheres,[7] quantum dots,[8] carbon nanoparticle[9] carbon nanotube,[10] graphene oxide,[11] MnO_2 nanosheet,[12] MoS_2[13] and WS_2 nanosheets[14] have been examined as good donors or acceptors in RET or PET pairs for biosensing and bioimaging either in long range resonance energy transfer (LrRET)[15] or not. It is generally argued that a FRET interaction may be the predominant pathway though a few reports suggest that the donor or acceptor interactions with small gold nanoparticles,[16] graphene oxide,[17] and carbon nanotubes[18] may involve NSET, PET, or both FRET and PET in these sensing systems.

In energy transfer systems, either FRET or NSET models are well-utilized to understand the energy transduction. Although FRET is a very effective and convenient technique, it has serious limitations regarding the distance and orientation of donor and acceptor.[19] Compared to the FRET, NSET is a more efficient quenching technique occurred with much more long distances, especially for interaction between dyes or QDs and metals or semiconductor.[20] Meanwhile, in nature, PET is a major process which have been shown to compete with RET when donor and acceptor proximities each other.[21] Thus, energy transfer with donors and acceptors can sometimes be complex and the photophysical interactions accounting for the RET (either FRET or NSET) and PET have not been clear. To achieve better design in biosensing, a more detailed understanding of RET and PET interactions, or the coupling of RET and PET (RET©PET), between traditional donor/acceptor and a wide array of electronically relevant acceptor/donor materials is required.

The chalcogenides semiconductor nanocrystals have drawn increasing attention for their interesting photophysical properties[22] and wide application.[23] They reveal intense and broad localized surface plasmon resonance (LSPR) spectra over UV to near infrared (NIR) wavelengths, suggesting the possibility of a RET interaction occurrence due to the spectral overlap between visible-emitting dyes.

However, the poor biocompatibility and difficult modification limit their common applications in biological applications. Inspired by the above findings, we assemble the binary $Cu_{2-x}SeNPs$ with the polydopamine ($Cu_{2-x}SeNPs$@pDA), which can form a conformal and continuous coating layer atop nearly various material present in the alkaline media. [24] Dopamine is redox active and its quinone structure naturally provides a better electron acceptor.[25] The photophysical interactions in the polydopamine-embedded $Cu_{2-x}SeNPs$@pDA nanostructures and dyes accounting for the possibility of RET in addition to PET may be warranted.

In such case, herein an efficient biosensing platform with RET©PET was developed for the first time by using ssDNA-conjugated fluorescent dyes (listed in Table S1) including TAMRA ($\lambda_{ex}/\lambda_{em}$, 540 nm/582 nm), Cy5 ($\lambda_{ex}/\lambda_{em}$, 630 nm/668 nm) and AMCA ($\lambda_{ex}/\lambda_{em}$, 353 nm/452 nm) and $Cu_{2-x}SeNPs$@pDA as the energy donor–acceptor pair. This strategy has been successfully exploited for the detection of specific DNA and proteins. Meanwhile, investigations on the energy transfer interactions between $Cu_{2-x}SeNPs$@pDA and dyes identified as a RET quenching mechanism, in which somewhat incongruous PET process involved. A detailed photophysical analysis suggested that the NSET (rather than FRET) and PET interactions (RET©PET) occurred in this sensing system. On the basis of the results by thorough characterization of the $Cu_{2-x}SeNPs$@pDA and dyes quenching using steady-state and time-resolved fluorescence, we further determined the competing rates for NSET and PET interactions, respectively.

Experimental

Apparatus

Transmission electron microscopy (TEM) measurements were obtained from a Tecnai G2 F20 S-TWIN microscopy (FEI, USA). The X-ray photoelectron spectroscopy (XPS) analysis was conducted by an ESCALAB 250 X-ray photoelectron spectrometer (Thermo, USA). The samples for XPS were made by the deposition of a nanocrystal suspension in water on Si substrate. Scanning electron microscopy (SEM) and Energy-dispersive X-ray spectroscopy (EDS) was performed with an S-4800 scanning electron microscope (Hitachi, Japan). A Fourier transform infrared (FT-IR) spectrophotometer (FTIR-8400S, Shimadzu, Japan) was employed to measuring the FT-IR spectrum. UV−vis−NIR absorption spectra were obtained using a Hitachi U-3600 spectrophotometer. Steady-state fluorescence spectra and fluorescence anisotropy were measured with an F-2500 fluorescence spectrophotometer (Hitachi, Japan) with the nanoparticles dispersed in reagents. Fluorescence lifetimes were measured by an FL-TCSPC fluorescence spectrophotometer (Horiba Jobin YvonInc., France) using a NanoLED laser light source at the respective excitation wavelength of the dyes. The data were fitted by a double-exponential decay model.

Reagents and materials

Copper sulfate ($CuSO_4 \cdot 5H_2O$, 99%) was purchased from Sinopharm Chemical Reagent Co., Ltd. (Shanghai, China). Selenious dioxide (SeO_2, 99.9%) and Bovine serum albumin (BSA) was obtained from Aladdin Chemistry Co. Ltd. (Shanghai, China). Polystyrene sulfonate (PSS, MW 70 kD) and vitamin C (Vc) were purchased from Alfa Aesar Co. Ltd. (MA, USA). Dopamine hydrochloride, thrombin and lysozyme were purchased from Sigma-Aldrich (Steinheim, Germany).

All oligonucleotides were purchased from Shanghai Sangon Biological Engineering Technology & Services Co., Ltd. (Shanghai, China). The nucleic acids were HPLC-purified and freeze-dried. Stock solutions of DNA were prepared with 10 mM PBS buffer, pH 7.4.

Preparation of $Cu_{2-x}Se$ and $Cu_{2-x}SeNPs$@pDA

The $Cu_{2-x}SeNPs$ were prepared by our previously developed simple wet chemical method with small modifications [23j]. Briefly, 2 mL of 10 mg mL^{-1} PSS and 13 mL water were added to a round-bottom flask, and then 0.5 mL 0.2 M SeO_2 and 1 mL 0.4 M Vc was added, successively. After 10 min, a mixed solution of 0.5 mL 0.4 M $CuSO_4 \cdot 5H_2O$ and 2 ml 0.4 M Vc were added under vigorous stirring at 30 ^oC. The resulting mixture was allowed to proceed under vigorous stirring at room temperature in 10 h until a green solution was obtained. The solution was centrifuged at 10000 rpm for 10 min and purified through a 10 kDa dialysis membrane for 24 hours with distilled water.

Polydopamine-embedded $Cu_{2-x}Se$ ($Cu_{2-x}SeNPs$@pDA) NPs were constructed by in situ polymerization of dopamine on $Cu_{2-x}Se$ surface according to refs with some modifications.[24] Shortly, 10 mL of the as-prepared $Cu_{2-x}Se$ suspension, were dispersed under continuous stirring in 50 mL of 2 mg mL^{-1} dopamine solution 1h to obtain $Cu_{2-x}SeNPs$@pDA (PBS, pH=8.5). The obtained $Cu_{2-x}SeNPs$@pDA was washed with water for 5 times to remove the unreacted dopamine and purified through a 10 kDa dialysis membrane for 24h. The product was stored in 4^oC fridge and kept for the application.

Quenching efficiency investigation

Different concentrations of $Cu_{2-x}SeNPs$@pDA were added to solutions containing various dyes-labeled ssDNA (P1, P3 and P4). In all cases, the total volume of the reaction solution was 500 μL. After incubation for 10 min, the fluorescence was measured by F-2500 fluorescence spectrophotometer.

Procedures for ssDNA detection

For ssDNA detection, 40 nM of P1 probe was first incubated with 1.25 mg L^{-1} $Cu_{2-x}SeNPs$@pDA at room temperature in a buffer solution respectively. After 10 min, different concentrations of target DNA were added to the sample solution. Then the mixture was incubated at 37 °C for 0.5 h, and the F-2500 fluorescence spectrophotometer was used to record the fluorescence intensity changes at emission wavelength of fluorescent dyes respectively.

Procedures for thrombin detection

40 nM of P2 probe was first incubated with 1.25 mg L^{-1} $Cu_{2-x}SeNPs$@pDA at room temperature in a buffer solution. After 10 min, different concentrations of thrombin were added to the sample solution. Then the mixture was incubated at 37°C for 0.5 h, and the F-2500 fluorescence spectrophotometer was used to record the fluorescence (FL) intensity change at fluorescent dyes exaction wavelength.

Resonance energy transfer

The efficiency of quenching (η_{total}) for steady-state PL quenching can be related to the excited-state donor lifetime τ, and this relationship can be written as,[19]

$$\eta_{total} = 1 - \frac{\tau_N}{\tau_0} \quad (1)$$

Wherein τ_N is the FL lifetime of the dyes labeled DNA with Cu_{2-x}SeNPs@pDA, while τ_0 is the dyes labeled DNA lifetime in the absence of Cu_{2-x}SeNPs@pDA.

A generic form of the efficiency of quenching allows the distance of separation between the donor and acceptor (r) and the R_0 (the 50% quenching distance) value to be solved, leading to power law distance dependence,[3]

$$\eta = \frac{1}{(1+(\frac{r}{R_0})^n)} \quad (2)$$

The exponent n is dependent on the nature of energy transfer. For FRET model, which is relative to interaction of two nearby oscillating dipoles, an n=6 distance-dependent quenching efficiency obeyed, while for NSET, which accounts for the formation of dipole-induced electron-hole pairs in a thin layer of a semi-infinite metal hemisphere, an n=4 distance dependence is expected to follow. For FRET model,

$$R_0 = 9.78\times10^3(\kappa^2 n^{-4} Q_{dye} J)^{1/6} \quad (3)$$

In which Q_{dye} is the quantum yield of the donor, while κ^2 is always 2/3,[26] n is the refractive index of the medium, and $J(\lambda)$ is the overlap integral between the donor emission and the acceptor absorption.

The theoretical value of NSET, namely d_0, can be calculated using the following expression as,

$$d_0 = (0.225\frac{c^3 Q_{dye}}{\omega_{dye}^2 w_F k_F})^{1/4} \quad (4)$$

Wherein ω_F is angular frequency and k_F is Fermi wavevector for Cu_{2-x}SeNPs@pDA; ω_{dye} and Q_{dye} represent the angular frequency of donor emission, and the quantum yield of the donor, respectively, and c is the speed of light.

The estimated NSET efficiency can also be defined using the expression:

$$\eta_{NSET} = \frac{k_{NSET}}{k_{total}} \quad (5)$$

Wherein k_{total} is the total decay rate and is equal to the inverse of the measured FL lifetime of the dyes in the presence of Cu_{2-x}SeNPs@pDA. The NSET rate constants (k_{NSET}) can then be determined by combining eqs 4 and 5.

NSET and PET kinetic analysis

The total decay rate k_{total} of the Cu_{2-x}SeNPs@pDA-dye labelled DNA complex is equal to the sum of all of the potential deactivation rates,[21d]

$$k_{total} = k_r + k_{nr} + k_{NSET} + k_{PET} = \frac{1}{\tau_N} \quad (6)$$

Where k_r is the radiative decay rate, k_{nr} is the nonradiative decay rate, k_{NSET} is the NSET rate and k_{PET} is the PET rate. Since

$$k_r + k_{nr} = \frac{1}{\tau_0} \quad (7)$$

$$k_{PET} = k_{total} - k_{NSET} - k_0 \quad (8)$$

And the PET efficiency can also be estimated as

$$\eta_{PET} = \frac{k_{PET}}{k_{total}} \quad (9)$$

Results and discussion

Characterization of Cu_{2-x}SeNPs@pDA

In this study, we used a simpler model system to develop an understanding of specific biosensing principle. Figure 1A provides a schematic depiction of the polydopamine-embedded Cu_{2-x}Se (Cu_{2-x}SeNPs@pDA) conjugates used along with the preparation steps involved. Cu_{2-x}SeNPs with the diameter of 40 nm were firstly synthesized according to our previously reported procedures,[23j] and the polydopamine-embedded Cu_{2-x}Se (Cu_{2-x}SeNPs@pDA) were constructed by in situ polymerization of dopamine on Cu_{2-x}Se surface.[24] Then the dyes-labelled DNA bound to the Cu_{2-x}SeNPs@pDA due to multiple catechol and amine interactions.[24b,c] The TEM imaging analysis (Figure 1B) revealed the Cu_{2-x}SeNPs were fully embedded, which was formed by pDA adherence with the thickness of 10 nm. The surface composition of Cu_{2-x}SeNPs@pDA has been validated by XPS (Figure 1C), whereas the elemental analysis determined by SEM-EDS (Figure 1S) with averaging among several particles showed an average Cu/Se atomic ratio of 1.74/1. Fourier transform infrared (FTIR) spectra (Figure S2) at 1045 cm^{-1} (C-O from vibrations benzene ring) and 1519 cm^{-1} (N-H scissoring vibrations) showed the

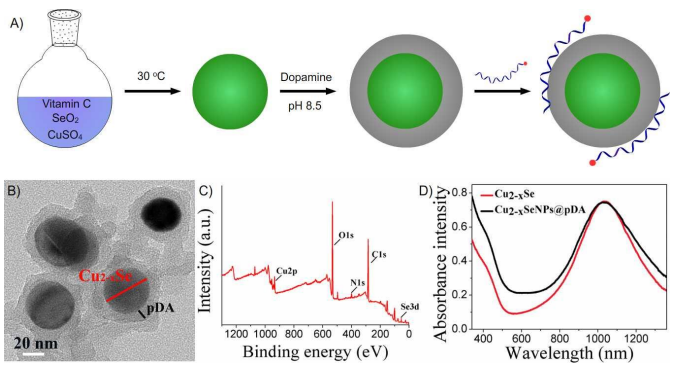

functional groups of dopamine on the surface of Cu_{2-x}SeNPs. Moreover, the extinction spectra Cu_{2-x}SeNPs@pDA show broad range over 200–1350 nm which have higher intensity than that of Cu_{2-x}SeNPs (Figure 1D)

Figure 1. Synthesis of polydopamine-embedded Cu_{2-x}Se and assembly of the Cu_{2-x}SeNPs@pDA with dyes-labelled DNA conjugates (A), the TEM image (B), the XPS scans of the synthesized Cu_{2-x}SeNPs@pDA (C) and the broad extinction spectra of Cu_{2-x}Se and Cu_{2-x}SeNPs@pDA (D).

Mechanism for the energy transfer and charge transfer analysis

It can be seen that the emission spectrum of dyes-labelled DNA (TAMRA-DNA, Cy5-DNA, AMCA-DNA,) could overlap with the absorption spectrum of Cu_{2-x}SeNPs@pDA to some extent (Figure 2A), suggesting that energy acceptor can be adaptable to diverse fluorophores emitting at different regions. While above analysis provided strong evidence that we can design DNA-conjugated fluorescent organic dyes acting as donors to construct the resonance energy transfer (RET) pairs with energy transfer acceptors of Cu_{2-x}SeNPs@pDA, some

other potential mechanisms still cannot be overlooked. Take the DNA-conjugated TAMRA for example, the energy levels for the $Cu_{2-x}SeNPs$@pDA relative to the lowest unoccupied molecular orbital (LUMO) of TAMRA (for derivation, the calculation can be seen in Supporting Information, calculation of the energy lever) can be obtained. The indirect band gap energies of $Cu_{2-x}SeNPs$ can be estimated to be 1.94 eV (Figure 2B) by the absorption spectrum, which was consistent with the previous reports.[22] And the valence and conduction band potential (E_{VB}/E_{CB}) were determined to be -5.86 / -3.92 eV relative to vacuum potential. The orbital energy for LUMO and the highest occupied molecular orbital (HOMO) of TAMRA and pDA was estimated by the B3LYP method in Dmol3 mode. As shown in Figure 2C, Photo-excited electrons in the TAMRA-DNA were energetically allowed photo-induced electron transfer (PET) from CB of $Cu_{2-x}Se$ and LUMO of the TAMRA to the LUMO of quinone structure of DA which was consistent with the reported results for the existence of quinone structure.[25] Overall, the possibility for the coupling of the RET and PET (RET©PET) can be provided by the spectral overlap and charge transfer energetically feasible in this system.

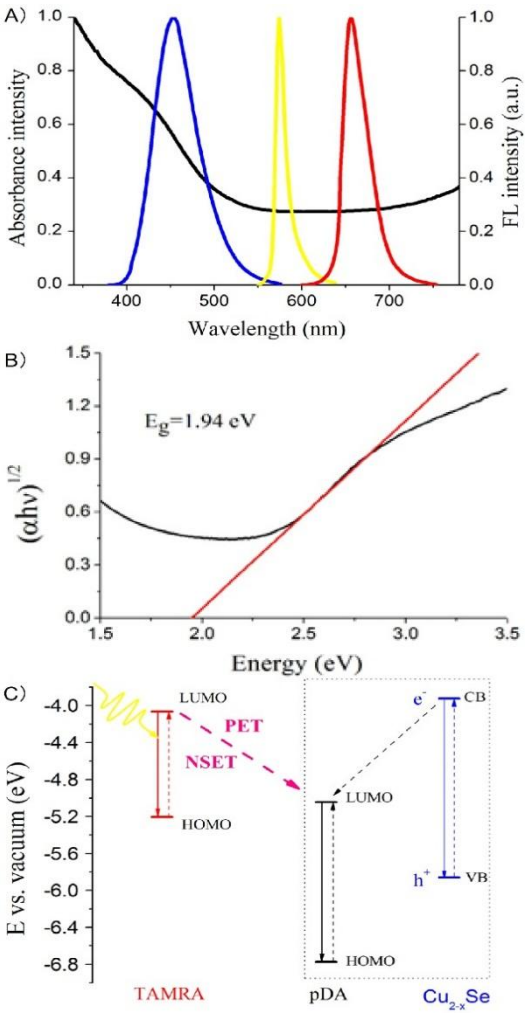

Figure 2. Schematic representation of possible energy transfer pathways. (A) Spectral overlap: normalized extinction spectra of $Cu_{2-x}SeNPs$@pDA (black) and emission spectra of the AMCA-DNA (blue), TAMRA-DNA (yellow) and Cy5-DNA (red). Note: only < 800nm absorbance shown for brevity and clearness. (B) The indirect band gap of $Cu_{2-x}SeNPs$ was calculated by the extinction spectra. (C) Schematic representation of $Cu_{2-x}Se$ conduction band (CB) and valence band (VB) relative to the quinone structure of DA and TAMRA lowest unoccupied molecular orbital (LUMO) along with putative pathways for both the NSET and PET quenching pathways.

Since data and theory supported the potential for both RET and PET quenching mechanisms, we should investigate the RET and PET contributions to the total coupling. And the RET process needed to be clear in the first place. RET process is strongly dependent on the distance between donor and acceptor, and successful application of energy transfer models (FRET or NSET) is required. Figure 3 revealed the fluorescence quenching. capability of the $Cu_{2-x}SeNPs$@pDA network with the dye-labelled ssDNA. Upon addition of $Cu_{2-x}SeNPs$@pDA into the solution of the dye-labelled ssDNA (P1, P3, P4), the fluorescence intensity greatly decreased (Figure 3A-C). The quenching efficiency of $Cu_{2-x}SeNPs$@pDA on the fluorescence of P1, P3, and P4 was 96.5%, 93.1% and 98.5%, respectively. Moreover, the fluorescence intensity could reached the steady value within only 3 min (Figure S4), indicating the fast quenching kinetics of fluorophore with $Cu_{2-x}SeNPs$@pDA. With the increasing $Cu_{2-x}SeNPs$@pDA concentration, the change of fluorescence intensity for dye-labelled ssDNA shown a Lineweaver−Burk plot (Figure 3D-E), while the Stern-Volmer plot[19,27] shown a relative poor correlation (Figure S5). These results indicated that the two quenching mechanism coexisted and the dynamic quenching seemed to act more importantly in these strategies especially for P1. In addition to steady-state analysis, Figure S6 displayed the kinetic traces of fluorophore-labelled DNA connecting with $Cu_{2-x}SeNPs$@pDA, respectively. The FL lifetimes was analysed with the software package, DataStation V2.4, and was fit by a sum of biexponential decay model,

$$F(t) = A_1 \exp(-\frac{t}{t_1}) + A_2 \exp(-\frac{t}{t_2}) \quad (10)$$

Where F(t) is the obtained kinetic decay curve, A_i is the amplitude of the ith decay channel and τ_i is the corresponding lifetime. Two exponentials were required to fit the decay data, thus, the average lifetime (listed in Table S2) was calculated using

$$t = \frac{A_1 t_1 + A_2 t_2}{A_1 + A_2} \quad (11)$$

Consistent with the steady-state results, the average fluorescence lifetimes (τ_{av}) decreased with the addition of $Cu_{2-x}SeNPs$@pDA. This increased contribution from the fast decay component was attributed to quenching of dyes-labelled DNA by the highest concentration of $Cu_{2-x}SeNPs$@pDA through energy and electron transfer and suggested considerable interaction between the two.[17] As $Cu_{2-x}SeNPs$@pDA concentrations increased, the number of free dyes-labelled DNA diminished, resulting in a smaller pre-exponential contribution of from the long decay component, τ_2. These results confirmed the strong interactive nature of dyes-labelled DNA toward $Cu_{2-x}SeNPs$@pDA.

TABLE 1 Relevant properties for Dyes and $Cu_{2-x}SeNPs$@pDA-dyes in NSET Process

Dyes	AMCA-DNA	TAMRA-DNA	Cy5-DNA
ω_{dye} (rad s^{-1}) [a]	4.17×10^{15}	3.24×10^{15}	2.82×10^{15}
ω_{NP} (rad s^{-1}) [b]	9.13×10^{15}	9.13×10^{15}	9.13×10^{15}

k_F (cm^{-1}) [b]	0.85×10^8	0.85×10^8	0.85×10^8
d_0 (Å)	68.5	84.4	70.4
r(Å) [c]	61.2	61.2	61.2

[a] determined with $2\pi c/\lambda_{em}$ by ref.3; [b] determined by LSPR modelling with Mie-Drude model in Supporting Information. [c] assuming ideal condition that the dyes separated from the NPs sphere by a rigid distance.

When the FRET based analysis for the RET, it showed that the R_0 values (Figure S7, Table S3) for the dyes donor and $Cu_{2-x}SeNPs$@pDA acceptor fall outside the range of the ruler for FRET (10-100 Å).[3] The quenching effect observed exceeded the traditional FRET model and this has motivated us to apply longer range "spectroscopic rulers"–the NSET model. For NSET, the large size of the metal nanoparticles and higher polarizability relative to the smaller fluorescent molecule produces longer range effects. As shown in Table 1, the predicted d_0 for 50% energy transfer efficiency is longer than the center-to-surface of the dye to $Cu_{2-x}SeNPs$@pDA separation distance (about 61.2 Å) based on a specific DNA conformation which showed the powerful quenching efficiency of the $Cu_{2-x}SeNPs$@pDA.

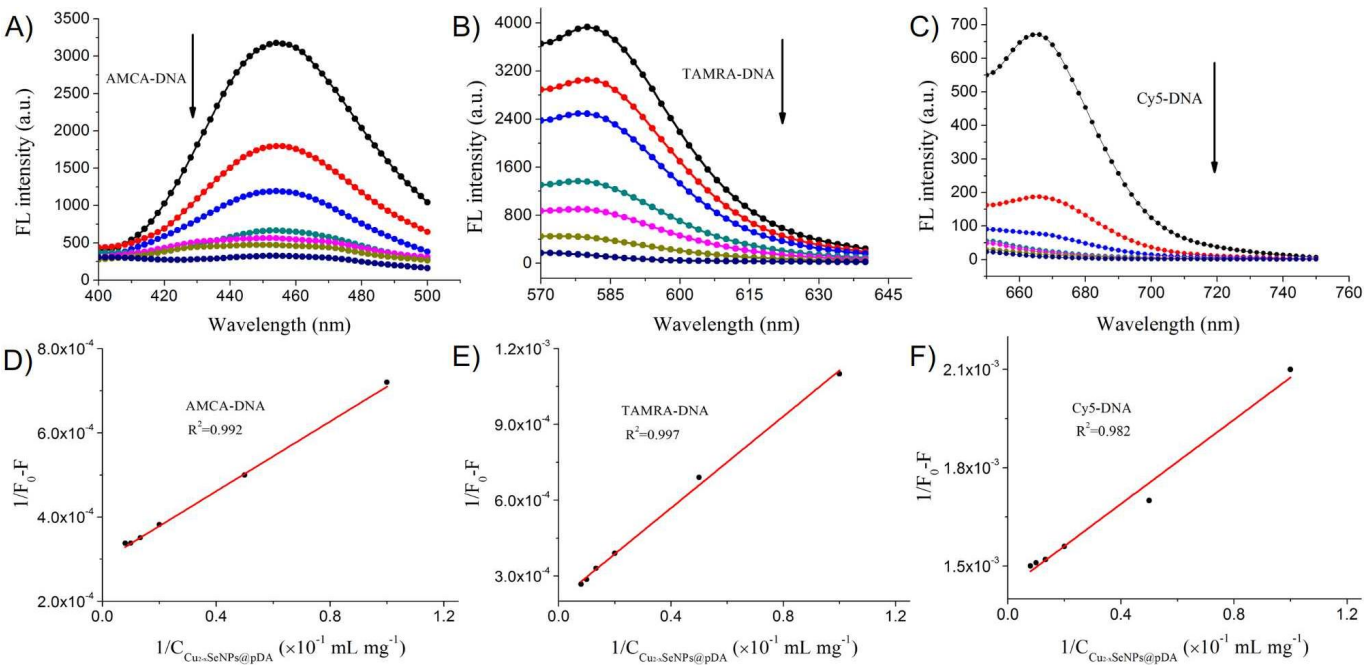

Figure 3. Control experiments to verify the dynamic quenching of three dyes-labelled DNA with $Cu_{2-x}SeNPs$@pDA. (A-C) Representative PL spectra collected from the emitting 40 nM dyes-labelled DNA assembled with the indicated increasing concentration of $Cu_{2-x}SeNPs$@pDA (0, 0.1, 0.2, 0.5, 0.75, 1, 1.25 mg L^{-1}) in PBS. (D-E) Lineweaver-Burk plots for the three dyes-labelled DNA quenching. F_0 and F are the fluorescence intensity of the fluorophore in the absence and presence of $Cu_{2-x}SeNPs$@pDA, respectively. λ_{em} (AMCA-DNA) = 452 nm, λ_{em} (TAMRA-DNA) = 582 nm, λ_{em} (Cy5-DNA) = 668 nm.

TABLE 2 Estimated the NSET and PET Rate Constants (s^{-1}) for $Cu_{2-x}SeNPs$@pDA-dyes Conjugates

k	k_{total}	k_{NSET} (η_{NSET})	k_{PET} (η_{PET})
AMCA-DNA	1.72×10^9	1.05×10^9(61.1%)	4.13×10^8(24.0%)
TAMRA-DNA	4.00×10^9	3.13×10^9(78.3%)	5.09×10^8(12.7%)
Cy5-DNA	1.43×10^{10}	9.11×10^9(63.7%)	4.55×10^9(31.8%)

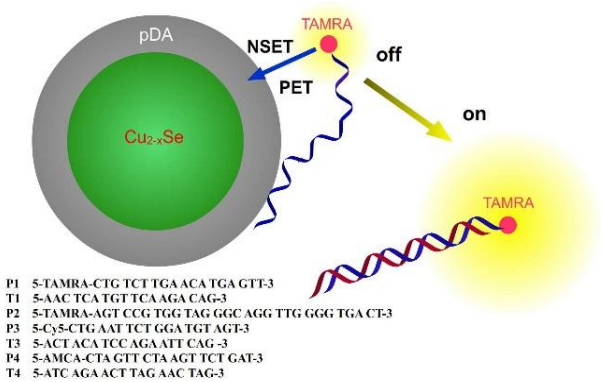

Figure 4. Schematic illustration of the fluorescence sensing of nucleic acid with $Cu_{2-x}SeNPs$@pDA as the quencher

When dyes-labelled DNA were assembled with $Cu_{2-x}Se$ coating without pDA that did not have favorable energy matching for charge transfer, only a relative minor amount of PL signal was quenched (< 80%) (Figure S8). When the FRET model was applied, the R_0=218 Å, r= 61.2 Å (centre-to-surface of the dye to $Cu_{2-x}SeNPs$ separation distance) and the energy transfer efficiency is close to 100%. It is deviated from the experimental results. While the NSET model was applied, R_0=84.4 Å, r= 61.2 Å, and the energy transfer efficiency was about 78%. It is more close to the experimental results. These results can help to confirm the energy transfer between $Cu_{2-x}SeNPs$@pDA and the dyes would be interpreted by NSET model rather than FRET model. And critically, it was further proved PL quenching with $Cu_{2-x}SeNPs$@pDA could be efficiently quenched owing to the RET and PET mechanism both. Since data and theory supported the potential for NSET©PET quenching mechanisms, we adopted a simple mathematical model to simulate the putative NSET and PET contributions to the total quenching observed for each dye when assembled with $Cu_{2-x}SeNPs$@pDA. Nano-second lifetime quenching studies were used to estimate the theoretical NSET and PET efficiency. The extract relevant RET and NSET rates were calculated and summarised in Table 2, assuming that RET and PET were the only relevant quenching mechanisms. Although both processes were permitted, NSET appeared to be more favored (especially when *r*<61.2 Å in actual experiment states as ssDNA would not show a rigid conformation) for sufficient spectral overlap.

Sensing platform for DNA and thrombin detection

The strategy based on the disclosed NSET and PET coupling for DNA detection can be shown in Figure 4. We use target DNA and thrombin detection as the model to evaluate the sensing ability. The aromatic nucleotide bases were assembled onto the plane network of $Cu_{2-x}SeNPs$@pDA via p–p stacking, van der Waals force and hydrophobic interaction. When the donor and the acceptor were taken into close proximity, it made the occurrence of RET©PET and "turned off" the fluorescence intensities of the donors (off-state). With the introduction of target molecular, the grid conformation of the nucleotide bases formed, which can reduce the exposure of the nucleobases, resulting in weaker interaction of the p–p stacking van der Waals force and hydrophobic interaction than that of ssDNA. As a consequence, the RET©PET process was inhibited, and led to a decrease in quenching effect (turn-on state). Therefore, a "turn-on" strategy sensor for analysis of multiple targets in homogeneous solution can be developed when different probes with corresponding fluorophores were used.

The effect of target DNA on the dyes-labelled DNA and the $Cu_{2-x}SeNPs$@pDA system has been investigated. As shown in Figure 5, when 40 nM tDNA (T1) were added to 40 nM P1 solution, its fluorescence intensity and peak location shown slight changes (curve a, b), which arised from the effect of primary and secondary structures of DNA on the fluorescence properties of labelled dyes.[13] The results implied that the interaction between dsDNA and NPs was much weaker than that between ssDNA and $Cu_{2-x}SeNPs$@pDA. However, when $Cu_{2-x}SeNPs$@pDA were added to the P1 solution, the fluorescence intensity of P1 was decreased verifying the RET and PET process between P1 and $Cu_{2-x}SeNPs$@pDA (curve c). Upon addition of 40 nM T1 to the P1/$Cu_{2-x}SeNPs$@pDA mixture solution for 30 min (Figure S9), the fluorescence intensity of the P1/$Cu_{2-x}SeNPs$@pDA system was recovered (curve d). This phenomenon showed that the affinity interaction

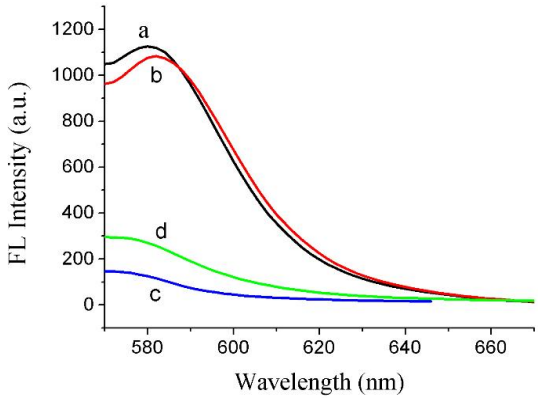

Figure 5. Fluorescence spectra of P1 (a, 40 nM) and P1/T1 (b, 40 nM) duplex in the absence and presence of $Cu_{2-x}SeNPs$@pDA (c:P1/$Cu_{2-x}SeNPs$@pDA and d: P1//T1$Cu_{2-x}SeNPs$@pDA).

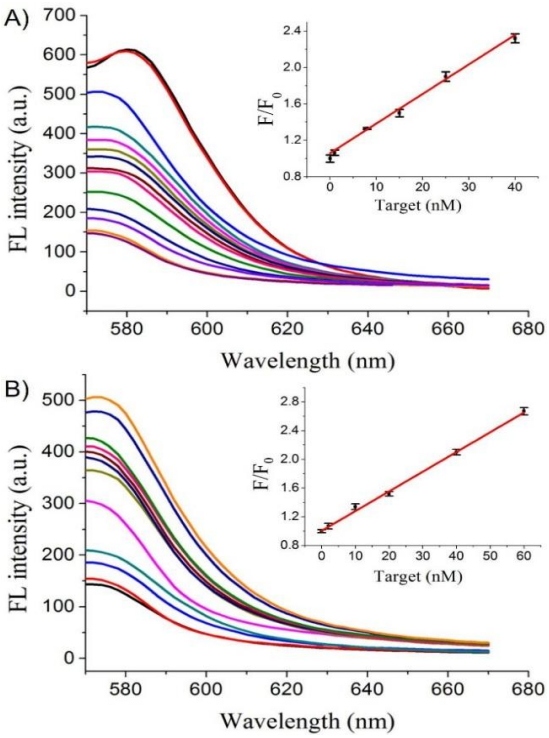

Figure 6. (A) Fluorescence spectra of the TAMRA-labelled DNA P1 (40 nM) in the presence of different concentrations of target DNA (0, 1, 8, 15, 25, 40, 60, 80, 100, 150, 250, 500, 800 and 1000 nM). Inset: calibration curve for target DNA T1 detection. (B) Fluorescence spectra of the TAMRA-labelled DNA P2 (40 nM) in the presence of different concentrations of target thrombin (0, 2, 10, 20, 40, 60, 100, 150, 250, 500, 800 and 1000 nM). Inset: calibration curve for target thrombin detection.

between complementary DNA single strand dramatically weakened the physical interaction between dsDNA and $Cu_{2-x}SeNPs$@pDA with the addition of target DNA. Therefore, the energy acceptors, $Cu_{2-x}SeNPs$@pDA, were separated away from the donors, resulting in the restoration of the fluorescence intensity of energy donors P1.

The feasibility of the binding state of the ssDNA with the $Cu_{2-x}SeNPs$@pDA network can be accessed via a study of fluorescence anisotropy (FA). As shown in Figure S10, the FA

value of P1 in an aqueous buffer solution was 0.035, and it increased to 0.29 after adding $Cu_{2-x}SeNPs$@pDA to the solution, indicating that the P1 was assembled onto the surface of NPs which restricted the rotation of the fluorophore. Thereafter, upon the addition of the target DNA (T1) that hybridized with the probe, the FA value was reduced back to 0.225, which suggested that the hybridization of P1 with the complementary target DNA effectively decreased the adsorption of P1 on the surface of $Cu_{2-x}SeNPs$@pDA. This result confirmed our above speculations.

The sensing platform was then applied to the detection of the target DNA (T1) with a homogeneous assay protocol. After introducing an increasing amount of the target sequence T1 to the sensing system, the emission of fluorophore was gradually recovered from the above-mentioned high efficiency of fluorescence quenching state (Figure 6A). And the plot of fluorescence intensity increment vs. T1 concentration showed a linear relationship in the concentration range from 1 to 40 nM (R^2 = 0.991). The detection limit was estimated at 3σ to be 0.5 nM.

We further looked into the specificity of the sensor using a series of contrast experiments and compared the fluorescence responses toward the target-DNA (T1), a single-base mismatched (SBM) sequence, and a noncomplementary (NC) sequence at the same concentration. As shown in Figure S11, the fluorescence recovery with 40 nM SBM DNA was much weaker than that obtained with the target T1, and the addition of 40 nM NC DNA caused nearly negligible alteration of the fluorescence intensity. The results demonstrated pronounced specificity of the sensor.

To demonstrate the universality of present proof-of-concept sensing system, a homogeneous model was adopted for thrombin analysis, just with thrombin binding aptamer as ssDNA. The results of FA for aptamer P2, P2/$Cu_{2-x}SeNPs$@pDA, P2/$Cu_{2-x}SeNPs$@pDA/thrombin (Figure S12) shown the feasibility to detect the target DNA with the protocol above. As shown in Figure 6B, we found that with increasing the concentration of thrombin from 0 to 1000 nM, the intensity enhanced accordingly. The inset showed the calibration curve for quantitative analysis of thrombin. The intensity was linearly dependent on the concentration of thrombin in the range from 2 to 60 nM, and the detection limit was 1 nM. Similarly, we demonstrated the selectivity of the aptamer sensor system. Biotin, lysozyme and BSA were chosen to investigate the selectivity. We found that thrombin could result in an obvious change in the fluorescence whereas other proteins lead to much weaker change (Figure S13). The results demonstrated the excellent selectivity of this approach applied in thrombin detection over competing proteins.

To demonstrate that broad-spectrum quenching capability, the multiplexed detection ability was further investigated. Three probes, P1, P3, and P4, labelled with TAMRA,Cy5, and AMCA, respectively were individually excited at 540, 630, and 353 nm, emitting yellow (582nm)，red (668 nm), and blue (452 nm) colours in these systems. The addition of target DNA of the corresponding fluorophore-labelled DNA probe into the P1/P2/P3/$Cu_{2-x}SeNPs$@pDA mixtures, resulting in significant fluorescence enhancement of the corresponding fluorophore significantly enhanced at the respective wavelength. When the mixture solutions containing different DNA targets were assayed, fluorescence intensity at all three emission wavelengths was intensified. With the addition of single target respectively, T1 enhanced the emission of P1 at 582 nm, T3 enhanced the emission of P3 at 668 nm, and T4 enhanced the emission of P4 at 452 nm (Figure S14A-C). The simultaneous detection of the two target DNAs was also carried out. When target T1 and target T4 were added to the mixed solution, the fluorescence enhancements for both TAMRA and AMCA channels were observed (Figure S14D). At the same time, the fluorescence intensity of P3 (Cy5 channel) did not change greatly. Moreover, when all three targets were present, fluorescence enhancements was observed in all three detection channels (Figure S14E). Although the multicolour quantitation in this network cannot be achieved for the interference of dyes with each other, these results showed that multicolour analysis of several oligonucleotides in homogeneous solution may be realized by the proposed sensing system.

Conclusions

The energy and charge transfer interactions between dyes-labelled DNA and $Cu_{2-x}SeNPs$@pDA have been systematically investigated. Combining steady-state and time-resolved fluorescence, we measured pronounced PL quenching for the dyes-$Cu_{2-x}SeNPs$@pDA assemblies. The NSET (rather than FRET) and PET interactions coupling (NSET©PET) were proved in this sensing system. The completing rates of the two mechanism were determined by the mathematic models. It showed that the NSET played more important role in these systems. Further studies will focus on the theoretical effect on different donors and the separation distance.

A homogeneous assay protocol for fluorescence signal-on platform between fluorescent probes and $Cu_{2-x}SeNPs$@pDA was developed. The synergy of the widespread LSPR of $Cu_{2-x}SeNPs$@pDA and the redox active dopamine made it be able to efficiently quench a variety of adjacent oligonucleotide-labelled dyes that emit over a wide wavelength range from the visible to NIR region. When the complementary target molecular was added, a weaker physical interaction between grid fluorescent probes and $Cu_{2-x}SeNPs$@pDA led to the recovery of fluorescence. Based on this features, the single target DNA had a dynamic range from 1 to 40 nM with a detection limit of 0.5 nM (S/N=3). We further successfully extended its application in proteins detection using aptamer–substrate as a model for thrombin detection in the linear range from 2 to 60 nM. And multicolour analysis of several oligonucleotides in homogeneous solution was also tested by the proposed sensing system, which demonstrated the potential application in the rapid screening of multi-targets with the polydopamine-embedded $Cu_{2-x}Se$ nanoparticles.

Acknowledgements

This study was financially supported by the National Natural Science Foundation of China (NSFC, Grant No. 21375109 and 21035005) and Chongqing Postdoctoral Science Foundation funded project (Xm2014021).

Notes and references

[a] *Key Laboratory of Luminescence and Real-Time Analytical Chemistry (Southwest University), Ministry of Education, College of Pharmaceutical Sciences, Southwest University, Chongqing, 400715, P. R. China, E-mail: chengzhi@swu.edu.cn, Tel: (+86) 23 68254659, Fax: (+86) 23 68367257.*

[b] *College of Chemistry and Chemical Engineering, Southwest University, Chongqing, 400715, P. R. China.*

† Electronic Supplementary Information (ESI) available: [details of any supplementary information available should be included here]. See DOI: 10.1039/b000000x/

1 A. R. Clapp, I. L. Medintz, J. M. Mauro, B. R. Fisher, M. G. Bawendi and H. Mattoussi, *J. Am. Chem. Soc.*, 2004, **126,** 301.

2 (a) T. Ozel, P. L. Hernandez-Martinez, E. Mutlugun, O. Akin, S. Nizamoglu, I.O. Ozel, Q. Zhang, Q. H. Xiong, and H. V. Demir, *Nano Lett.*, 2013,**13**, 2296; (b) H. J. Chen, L. Shao, K. C. Woo, J. F. Wang and H. Q. Lin, *J. Phys. Chem. C*, 2012, **116**, 14088;(c) M. Li, S. K. Cushing and N.Q. Wu, *Analyst*, 2015, **140**, 386.

3 (a) C. S. Yun, A. Javier, T. Jennings, M. Fisher, S. Hira, S. Peterson, B. Hopkins, N. O. Reich and G. F. Strouse, *J. Am. Chem. Soc.*, 2005, **127**, 3115; (b) M. P. Singh and G. F. Strouse, *J. Am. Chem. Soc.*, 2010, **132**, 9383.

4 Y. Liu, X. Dong and P. Chen, *Chem. Soc. Rev.*, 2012, **41**, 2283.

5 (a) D. J. Maxwell, J. R. Taylor and S. Nie, *J. Am. Chem. Soc.*, 2002, **124**, 9606; (b) D. A. Giljohann, D. S. Seferos, W. L. Daniel, M. D. Massich, P. C. Patel and C. A. Mirkin, *Angew. Chem., Int. Ed.*, 2010, **49**, 3280; (c) Y. Wang, X. H. Liu, J. L. Zhang, D. Ailiac and B. Liedberg, *Chem. Sc*i., 2014, **5**, 2651; (d) T. Ming, L. Zhao, H. J. Chen, K. C. Woo, J. F. Wang, and H. Q. Lin, *Nano Lett.*, 2011, **11**, 2296;(d) R. Ban, E. S. Abdel-Halim, J. R. Zhang and J. J. Zhu , *Analyst*, 2015, DOI: 10.1039/c4an02161d

6 H. F. Dong, J. P. Lei, H. X. Ju, F. Zhi, H. Wang, W. J. Guo, Z. Zhu, and F. Yan. *Angew. Chem. Int. Ed.*, 2012, **51**, 4607.

7 W. B. Qiang, W. Li, X. Q. Li, X. Chen and D. K. Xu, *Chem. Sci.*, 2014, **5**, 3018.

8 L. Zhang, R. Zhang, P. Cui, W. F. Cao and F. Gao, *Chem. Commun.*, 2013, **49**, 8102; (b) J. Ji, Y. Y. Shen, P. P. Hu, X. H..Li, L. P. Jiang, J. R. Zhang, L. L. Li and J. J. Zhu, *Anal. Chem.*, 2014, **86**, 3284; (c) S. Liu, W.D. Na, S. Pang, F.P. Shi and X.G. Su, *Analyst, 2014,* **139**, 3048.

9 X. Y. Ouyang, J. H. Liu, J. S. Li and R. H. Yang. *Chem. Commun.*, 2012, **48**, 88.

10 (a) R. H. Baughman and A. A. Zakhidov, W and A. de Heer, *Science* 2002, **297**, 787; (b) R. H. Yang, J. Y. Jin, Y. Chen, N. Shao, H. Z. Kang, Z. Y. Xiao, Z. W. Tang, Y. R. Wu, Z. Zhu and W. H. Tan, *J. Am. Chem. Soc.*, 2008, **130**, 8351;(c) S. J. Zhen, L. Q. Chen; S. J. Xiao, Y. F. Li, P. P. Hu, L. Zhan, L. Peng, E. Q. Song and C. Z. Huang, *Anal. Chem.*, 2010, **82**, 8432.

11 (a) L. Cui, Y. L. Song, G. L. Ke, Z. C. Guan, H. M. Zhang, Y. Lin, Y. S. Huang, Z. Zhu, and C. Y. Yang, *Chem.-Eur. J.*, 2013, **19**, 10442; (b) H. J. Zhang, S. Si , M. Lv, J. Y. Shi, X. L. Zuo, S. Su, L. H. Wang, W. Huang, C. H. Fan and Q. Huang, *Anal. Chem.*, 2013, **85**, 1424; (c) M. Yi, S. Yang, Z. Y. Peng, C. H. Liu, J. S. Li, W. W. Zhong, R. H. Yang and W. H. Tan, *Anal. Chem.*, 2014, **86**, 3548.

12 Y. X. Yuan, S. F. Wu, F. Shu and Z. H. Liu, *Chem. Commun.*, 2014, **50**, 1095.

13 C. F. Zhu, Z. Y. Zeng, H. Li, F. Li, C. H. Fan, and H. Zhang, *J. Am. Chem. Soc.*, 2013, **135**, 5998.

14 Q. Xi, D. M. Zhou, Y. Y. Kan, J. Ge, Z. K. Wu, R. Q. Yu, and J. H. Jiang, *Anal. Chem.*, 2014, **86**, 1361-1365.

15 (a) P. P. Hu, L. Q. Chen, C. Liu, S. J. Zhen, S. J. Xiao, L. Peng, Y. F. Li and C. Z. Huang, *Chem. Commun.*, 2010, **46**, 8285; (b) Y. Zhang, Y. Liu, S. J. Zheng and C. Z. Huang, *Chem. Commun.*, 2012, **47**, 8285.

16 (a) X. Zhang, C. A. Marocico, M. Lunz, V. A. Gerard, Y. K. Gun'ko, V. Lesnyak, N. Gaponik, A. S. Susha, A. L. Rogach and A. L. Bradley, *ACS Nano*, 2012, **6**, 9283; (b) X. Zhang, C. A. Marocico, M. Lunz, V. A. Gerard, Y. K. Gun'ko, V. Lesnyak, N. Gaponik, A. S. Susha, A. L. Rogach and A. L. Bradley, *ACS Nano*, 2014, **8**, 1273.

17 I. V. Lightcap and P. V. Kamat, *J. Am. Chem. Soc.*, 2012, **134**, 7109.

18 (a) J. E. Weaver, M. R. Dasari, A. Datar, Saikat Talapatra and P. Kohli, *ACS Nano*, 2010, **4**, 6883; (b) Q. B.Wang, W. W, J. P. Lei, N. Xu, F. L. Gao and H. X. Ju, *Anal. Chem.*, 2013, **85**, 12182.

19 J. R. Lakowicz, *Principles of Fluorescence Spectroscopy*, 3rd ed.; Springer: New York, 2006.

20 P. C. Ray, Z. Fan, R. A. Crouch, S. S. Sinha and A. Pramanik, *Chem. Soc. Rev.*, 2014, **43**, 6370.

21 (a) A. Boulesbaa, A. Issac, D. Stockwell, Z. Huang, J. Huang, J. Guo and T. Lian, *J. Am.Chem. Soc.*, 2007, **129**, 15132; (b) L. Qian, Y. Zheng, J. G. Xue and P. H. Holloway, *Nat. Photonics*, 2011, **5**, 543; (c) M. H. Stewart, A. L. Huston, A. M. Scott, A. L. Efros, J. S. Melinger, K. B. Gemmill, J. B. Blanco-Canosa, P. E. Dawson and I. L. Medintz, *ACS Nano*, 2012, **6**, 5330; (d) M. H. Stewart, A. L. Huston, A. M. Scott, E. Oh, W. R. Algar, J. R. Deschamps, K. Susumu, V. Jain, D. E. Prasuhn, J. Blanco-Canosa, P. E. Dawson and I. L. Medintz, *ACS Nano*, 2013, **7**, 9489.

22 (a) F. Scotognella, G. Della Valle, A. R. Srimath Kandada, D. Dorfs, M. Zavelani-Rossi, M. Conforti, K. Miszta, A. Comin, K. Korobchevskaya, G. Lanzani, L. Manna and F. Tassone, *Nano Lett.*, 2011, **11**, 4711; (b) Y. Zhao, H. Pan, Y. Lou, X. Qiu, J. Zhu and C. Burda, *J. Am. Chem. Soc.*, 2009, **131**, 4253; (c) A. Comin and L. Manna, *Chem. Soc. Rev.*, 2014, **43**, 3957.

23 (a) J. M. Luther, P. K. Jain, T. Ewers and A. P. Alivisatos, *Nat. Mater.*, 2011, **10**, 361; (b) C. M. Hessel, V. P. Pattani, M. Rasch, M. G. Panthani, B. Koo, J. W. Tunnell and B. A. Korgel, *Nano Lett.*, 2011, **11**, 2560; (c) X. Liu, C. Lee, W. C. Law, D. Zhu, M. Liu, M. Jeon, J. Kim, P. N. Prasad, C. Kim and M. T. Swihart, *Nano Lett.*, 2013, **13**, 4333; (d) X. Liu, Q. Wang, C. Li, R. Zou, B. Li, G. Song, K. Xu, Y. Zheng and J. Hu, *Nanoscale*, 2014, **6**, 4361; (e) J. L.Yue, Q. Sun and Z. W. Fu, *Chem Commun.*, 2013, **49**, 586; (f) X. Liu, X.Wang, B. Zhou, W. C. Law, A. N. Cartwright and M. T. Swihart, *Adv. Funct. Mater.*, 2013, **23**, 1256; (g) G. J. Xiao, Y. Zeng, Y. Y. Jiang, J. J. Ning, W. T. Zheng, B. B. Liu, X. D. Chen, G. T. Zou and B. Zou, *Small***,** 2013, **9**, 793; (h) S. Q. Lie, H. Y. Zou,Y. C. and C. Z. Huang, *RSC Adv.*, 2014, **4**, 55094; (i) W. L. Li, S. Q. Lie, Y. Q. Du, X. Y. Wan, T. T. Wang, J. Wang and Cheng Zhi Huang, *J. Mater. Chem. B*, 2014, **2**, 7027; (j) S. Q. Lie, D. M. Wang, M. X. Gao and C. Z. Huang, *Nanoscale*, 2014, **6**, 10289.

24 (a) H. Lee, S. M. Dellatore, W. M. Miller, P. B. Messersmith, *Science*, 2007, **318**, 426; (b) H. Lee, J. Rho and P. B. Messersmith, *Adv. Mater.*, 2009, **21**, 431; (c) H. O. Ham, Z. Q. Liu, K. H. Aaron Lau, H. Lee, and P. B. Messersmith, *Angew. Chem. Int. Ed.*, 2011, **50**, 732.

25 (a) S. J. Clarke, C. A. Hollmann, Z. J. Zhang, D. Suffern, S. E. Bradforth, N. M. Dimitrijevic, W. G. Minarik and J. L.Nadeau, *Nat. Mater.*, 2006, **5**, 409; (b) X. Ji, G. Palui, T. Avellini, H. B. Na, C. Y. Yi, K. L. K. Jr and H. Mattoussi, *J. Am. Chem. Soc.*, 2012, **134**, 6006.

26 L. Stryer, *Annu. Rev. Biochem.*, 1978, **47**, 819.

27 R. Hu, T. Liu, X.B. Zhang, S.Y. Huan, C. C Wu, T. Fu, and W. H. Tan, *Anal. Chem.*, 2014, **86**, 5009.